Heliyon 10 (2024) e23340

Contents lists available at ScienceDirect

Heliyon

journal homepage: www.cell.com/heliyon

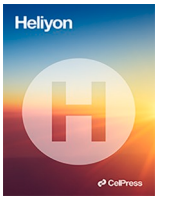

A ROI-based quantitative pipeline for ^{18}F-FDG PET metabolism and pCASL perfusion joint analysis: Validation of the ^{18}F-FDG PET line

Valeria Cerina [a,*], Cinzia Crivellaro [b], Sabrina Morzenti [c], Federico E. Pozzi [a,d,e], Vittorio Bigiogera [f], Lorenzo Jonghi-Lavarini [f], Rosa M. Moresco [f], Gianpaolo Basso [e,f,g], Elisabetta De Bernardi [f]

[a] PhD program in Neuroscience, School of Medicine and Surgery, University of Milano-Bicocca, Italy
[b] Nuclear Medicine, Fondazione IRCCS San Gerardo dei Tintori, Monza, Italia
[c] Medical Physics, Fondazione IRCCS San Gerardo dei Tintori, Monza, Italia
[d] Neurology, Fondazione IRCCS San Gerardo dei Tintori, Monza, Italia
[e] Milan center for Neuroscience (NeuroMI), University of Milano-Bicocca, Italy
[f] School of Medicine and Surgery, University of Milano-Bicocca, Italy
[g] Neuroradiology, Fondazione IRCCS San Gerardo dei Tintori, Monza, Italia

ARTICLE INFO

Keywords:
Dementia
Mild cognitive impairment
Brain 18F-FDG PET
Arterial spin labeling
ROI-Based quantitative analysis
Statistical parametric mapping (SPM)

ABSTRACT

In Mild Cognitive Impairment (MCI), the study of brain metabolism, provided by 18F-Fluoro-DeoxyGlucose Positron Emission Tomography (^{18}F-FDG PET) can be integrated with brain perfusion through pseudo-Continuous Arterial Spin Labeling Magnetic Resonance sequences (MR pCASL). Cortical hypometabolism identification generally relies on wide control group datasets; pCASL control groups are instead not publicly available yet, due to lack of standardization in the acquisition parameters. This study presents a quantitative pipeline to be applied to PET and pCASL data to coherently analyze metabolism and perfusion inside 16 matching cortical regions of interest (ROIs) derived from the AAL3 atlas. The PET line is tuned on 36 MCI patients and 107 healthy control subjects, to agree in identifying hypometabolic regions with clinical reference methods (visual analysis supported by a vendor tool and Statistical Parametric Mapping, SPM, with two parametrizations here identified as SPM-A and SPM-B). The analysis was conducted for each ROI separately. The proposed PET analysis pipeline obtained accuracy 78 % and Cohen's κ 60 % vs visual analysis, accuracy 79 % and Cohen's κ 58 % vs SPM-A, accuracy 77 % and Cohen's κ 54 % vs SPM-B. Cohen's κ resulted not significantly different from SPM-A and SPM-B Cohen's κ when assuming visual analysis as reference method (p-value 0.61 and 0.31 respectively). Considering SPM-A as reference method, Cohen's κ is not significantly different from SPM-B Cohen's κ as well (p-value = 1.00). The complete PET-pCASL pipeline was then preliminarily applied on 5 MCI patients and metabolism-perfusion regional correlations were assessed. The proposed approach can be considered as a promising tool for PET-pCASL joint analyses in MCI, even in the absence of a pCASL control group, to perform metabolism-perfusion regional correlation studies, and to assess and compare perfusion in hypometabolic or normo-metabolic areas.

* Corresponding author.
E-mail address: v.cerina2@campus.unimib.it (V. Cerina).

https://doi.org/10.1016/j.heliyon.2023.e23340
Received 29 September 2023; Accepted 1 December 2023
Available online 7 December 2023
2405-8440/© 2023 The Authors. Published by Elsevier Ltd. This is an open access article under the CC BY-NC-ND license (http://creativecommons.org/licenses/by-nc-nd/4.0/).

1. Introduction

^{18}F-FDG Positron Emission Tomography (PET) has been shown to provide useful information in the etiological diagnosis of different neurodegenerative dementias, and it has been deemed central in the workup of mild cognitive impairment in recent Italian and European consensus papers [1,2]. On the other hand, magnetic resonance imaging (MRI) is usually the first and most available tool to assess patients with cognitive complaints [1]. While FDG-PET provides data about cerebral metabolism, MRI has been traditionally used to evaluate structural properties, such as atrophy patterns. The recently introduced pseudo-Continuous Arterial Spin Labeling sequence (pCASL) can integrate MRI with functional data about brain perfusion without the need for contrast enhancement [3,4].

A few studies compared ^{18}F-FDG PET and pCASL in neurodegenerative dementias and healthy subjects [5–16]. In most of them, the principal aim is to assess the validity of the pCASL technique, and a general correlation has been found between perfusion and metabolism values [5,6,9,15,16]. However, the great heterogeneity among studies currently limits the translation of pCASL into clinical practice for patients with dementia. In particular, little attention has been given to the potential role of pCASL in the management of MCI patients.

In order to better understand the role of pCASL perfusion analysis in the diagnostic workup of cognitive decline, as a functional tool complementary or even alternative to ^{18}F-FDG PET, quantitative studies coherently analyzing PET and pCASL images on MCI patients are needed. PET cortical hypometabolism is commonly quantified with the SPM toolbox (https://www.fil.ion.ucl.ac.uk/spm/), that identifies pathological patterns by statistically comparing patient data with a control group (normative data). Multicentric normative data are made available e.g. by the Italian Association of Nuclear Medicine and Molecular Imaging (AIMN, https://www.aimn.it/). Since pCASL technique is not yet standardized among centers and vendors [17], perfusion images still depend on acquisition parameters, such as post-labeling delay or slab thickness. A few research groups have built internal small datasets of healthy subjects pCASL images, acquired by using different parameters [7,9]. However, large pCASL control groups are not publicly available yet, limiting the possibility of performing a PET-like SPM voxel-wise analysis.

To jointly analyze metabolism and perfusion in matching cortical areas in MCI patients, we developed a region of interest (ROI)-based quantitative analysis pipeline to be independently and coherently applied to PET and pCASL data. ROI-based quantitative analysis pipelines have been already applied in studies looking for PET-pCASL regional correlations in normal subjects, autosomal dominant Alzheimer and frontotemporal dementia patients [5,9,16]. The aim of this work is to tune and validate the pipeline on the PET line, where normative data can be exploited, in order to individuate hypometabolic regions in agreement with SPM conventional analysis and with the visual analysis of an expert nuclear medicine physician. The idea is that a regional PET-pCASL analysis tool that identifies hypometabolic areas could become a driver to interpret pCASL images, even in the absence of a pCASL control group. The pipeline results could indeed be used in metabolism-perfusion regional correlation studies, but also to assess and compare perfusion in areas identified by FDG-PET as hypometabolic or normal.

The work is organized as follows. The first part aims to describe the PET-pCASL pipeline. In the second part, the PET line is tuned and validated on a group of 36 MCI patients ^{18}F-FDG PET images to agree with SPM conventional analysis and with the visual analysis of an expert nuclear medicine physician supported by a vendor semi-quantitative tool. The third part aims to complete the PET-pCASL pipeline with PET normality ranges and apply it to a pilot group of MCI patients to assess metabolism-perfusion regional correlations.

2. Materials and methods

2.1. Study participants

MCI patients were recruited at the memory clinic of the Neurology Unit at Fondazione IRCCS San Gerardo dei Tintori under the CAPE-MCI protocol (ClinicalTrials ID NCT05756270). The protocol, approved by the Fondazione IRCCS San Gerardo dei Tintori Ethics Committee in accordance with the Declaration of Helsinki guidelines and with standards of good clinical practice (D.M. Sanità July 15, 1997 and s.m.i.), is part of an ongoing study aiming at exploring pCASL as a diagnostic and prognostic biomarker in the MCI workup. Inclusion criteria were MCI diagnosis according to clinical criteria by Petersen and subsequent modifications [18,19], with a Clinical Dementia Rating Extended Scale (CDR) score of 0.5. Subjects underwent neuropsychological tests, ^{18}F-FDG PET/CT, and MRI with pCASL sequence within a month, to minimize possible differences due to disease progression. A subset of patients also underwent lumbar puncture for the assessment of amyloid-beta, phosphorylated tau, and total tau, within the following 6 months.

The PET line is tuned and validated on the first 36 MCI patients that underwent the CAPE-MCI protocol, 18 males and 18 females aged 58–80 years (mean ± standard deviation: 72 ± 7 years). The entire PET-pCASL pipeline is applied and metabolism-perfusion regional correlations are computed on 5 MCI patients, 2 males and 3 females (mean and standard deviation: 74 ± 5). All the considered images passed a visual quality check, so they are free of artifacts (e.g., motion artifacts).

2.1.1. ^{18}F-FDG PET image acquisition and reconstruction

All MCI subjects underwent PET imaging with ^{18}F-FDG at Nuclear Medicine Department of Fondazione IRCCS San Gerardo dei Tintori, on GE Discovery IQ or GE Discovery MI PET/CT scanner, with 3D acquisition mode according to the standard European Association of Nuclear Medicine (EANM) protocol [20]. PET acquisition was performed after at least 6 h of fasting, with glycemia <160 mg/dL. About 125–250 MBq of ^{18}F-FDG were administered and acquisitions were performed 45–60 min after radiotracer injection, according to EANM guidelines. PET data acquisition lasted 10 min and images were reconstructed using an ordered subset expectation maximization (OSEM) algorithm with attenuation and scatter correction on a 256 x 256 matrix (pixels size = 1.17 mm ×

1.17 mm) with a slice thickness of 3.26 mm. Images were then smoothed with a 4 mm Gaussian kernel. All images were evaluated before analysis for patient motion and adequacy of statistical counts.

2.1.2. MR pCASL image acquisition protocol

MRIs were acquired on a 3.0 T Philips Ingenia CX (Philips Medical Systems Nederland B.V. of Eindhoven) equipped with a 32-channel head coil, at Neuroradiology Department of Fondazione IRCCS San Gerardo dei Tintori. MR data acquisition lasted 30 min. Whole brain structural MR images were acquired using volumetric magnetization prepared rapid gradient-echo sequence (MPRAGE; TR/TE/TI = 2300/2.98/900 ms, flip angle = 9°). The field of view was 240 mm × 256 mm, with 1 mm × 1 mm in plane resolution and 1 mm slice thickness. Perfusion images were acquired using a 3D pCASL sequence with a single-shot echo-planar imaging (EPI) readout, TR/TE = 2500/11 ms, post-labeling delay = 2000 ms, number of slices = 40, slice thickness = 4 mm, center to center distance = 7.2 mm, and in-plane resolution = 4 mm x 4 mm.

2.2. Proposed ROI-based quantitative analysis pipeline

The region of interest (ROI)-based quantitative analysis pipeline was implemented by means of the SPM12 toolbox, running in Matlab2022a (https://www.mathworks.com). Pre-processing and analysis steps have been coherently and specifically designed for PET and pCASL images, both characterized by scarce image quality [21]. The pipeline is shown in Fig. 1. It includes reorientation, spatial normalization in a common space, image quality enhancement, ROIs definition, and quantification. Some steps have been specifically adapted for PET and pCASL, e.g. PET images were directly normalized through the SPM12 default Tissue Probability Map (TPM), while pCASL normalization exploited associated T1-weighted structural images and source images.

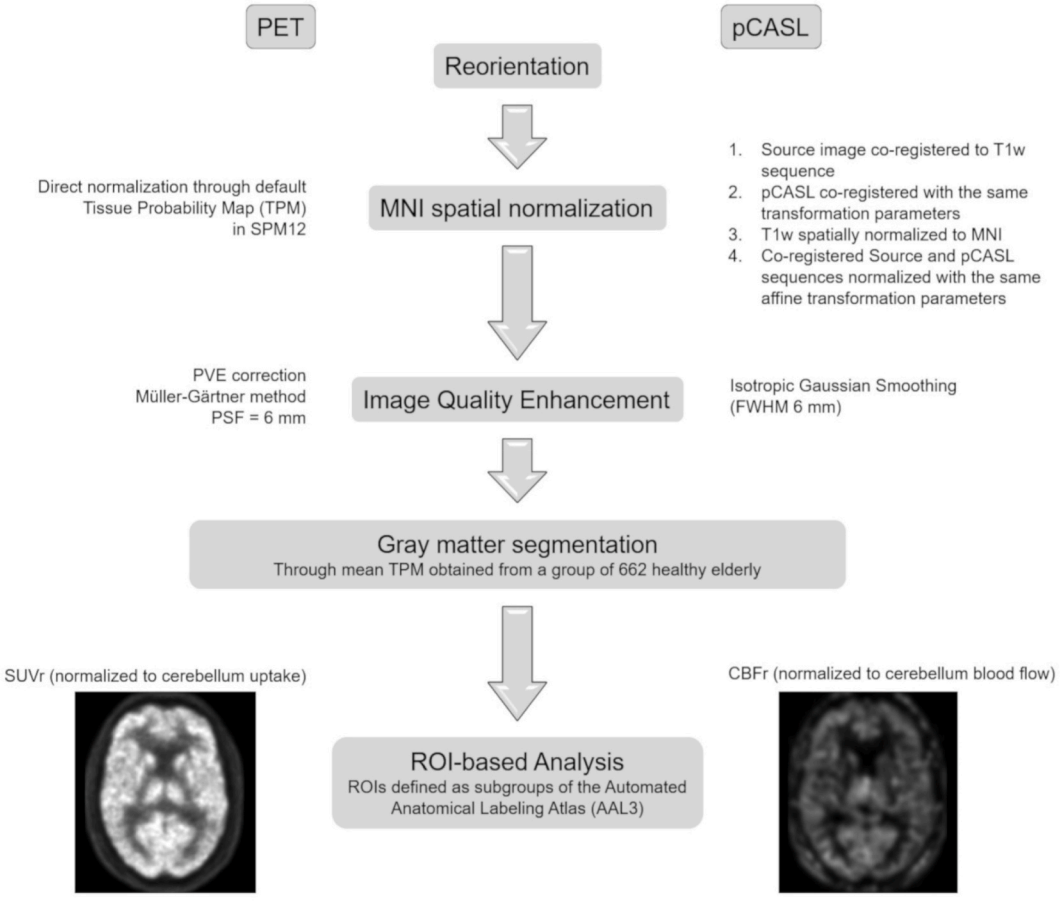

Fig. 1. Proposed analysis pipeline, developed in parallel and adapted for PET and pCASL. Reorientation as starting point for both sides. MNI normalization and image quality enhancement steps were adapted in parallel for PET and pCASL. Gray matter segmentation is obtained through a mean Tissue Probability Map (TPM) [Lemaître H. et al., 2005]. Standardized Uptake Values and Cerebral Blood Flow Values, both normalized to cerebellum uptake and blood flow respectively (SUVr and CBFr) are obtained for each Region of Interest (ROI) as average among all voxels.

2.2.1. Image pre-processing

After a reorientation phase, scans were spatially normalized through affine transformation into a common Montreal Neurological Institute (MNI)-152 atlas anatomical space and interpolated on a 1 x 1 × 1 mm^3 voxel grid. PET images were directly normalized through SPM12 TPM. To normalize pCASL scans, the control image M0 was first co-registered to the structural T1-weigthed (T1w) image and pCASL was accordingly co-registered. The T1w scan was then normalized in MNI space through SPM12 TPM. pCASL image was accordingly normalized to MNI space with T1w affine transformation parameters. Indeed, aware of pCASL low quality, a more reliable common space normalization can be obtained exploiting structural images [22]. Image quality enhancement for pCASL images was conducted through an isotropic Gaussian smoothing (FWHM = 6 mm). PET images, in the gray matter (GM) area, were corrected for partial volume effect (PVE) by means of the Müller-Gärtner partial volume correction (MG PVC) method [23] implemented in the petpve12 toolbox [24] with PSF = 6 mm. GM, white matter (WM), and cerebrospinal fluid (CSF) probability maps for PVE correction were obtained using a mean TPM constructed on a group of 662 healthy elderlies in the same age range as our patients [25]. More information about image quality enhancement choices can be found in the Discussion. GM area segmentation for PET and pCASL regional quantification was obtained from the same TPM with a threshold of 20 % [26,27].

2.2.2. Image analysis

Sixteen cortical ROIs were defined as subgroups of the Automated Anatomical Labeling Atlas version 3 (AAL3) from the CAT12 toolbox of SPM12, masked on the mean GM TPM as well. Regions characterized by an altered metabolism in the early phases of the most common neurodegenerative dementia (Alzheimer's disease, Lewy bodies dementia, and Fronto-temporal dementia) were selected, i.e., Posterior Cingulum, Occipital Cortex, Inferior Parietal Cortex, Superior Parietal Cortex, Precuneus, Lateral Prefrontal Cortex, Lateral Temporal Cortex and Mesial Temporal Cortex [18,20,28–31]. Mesial temporal and parietal hypometabolism on ^{18}F-FDG PET imaging may predict clinical progression of elderly normal into mild cognitive impaired subjects [31]. Thus, the areas selected included the main areas involved in AD (such as posterior cingulum, precuneus, parietal and temporal regions). However, different patterns of hypometabolism have been found to predict the progression of specific cognitive deterioration corresponding to different neurodegenerative substrates, showing heterogeneous hypometabolic profiles among MCI subjects [31]. Thus, also the frontal and occipital cortex were included. On ^{18}F-FDG PET images, average Standardized Uptake Values (SUV) were computed inside each ROI and normalized with respect to the cerebellum average SUV to obtain SUV ratios (SUVr). On MR pCASL images, average Cerebral Blood Flow values (CBF) were computed inside each ROI and normalized with respect to the cerebellum average CBF to obtain CBF ratios (CBFr).

2.3. Validation and tuning of the PET line

2.3.1. ^{18}F-FDG PET healthy control dataset

An ^{18}F-FDG PET dataset of 107 healthy subjects was collected as control group. 84 healthy scans came from the AIMN database (https://www.aimn.it/site/page/gds/gds-5) and 23 healthy subjects were collected from an internal database [32]. Globally, the healthy control group included 53 males and 54 females, with a mean age of 69 (±6) years. Healthy control group ^{18}F-FDG PET scans were comparable to MCI subjects' scans in terms of acquisition parameters and reconstruction methods.

2.3.2. Normality range definition

On the healthy control group, SUVr means and standard deviation (σ) for each ROI were computed. For the analysis of patient regional hypometabolism, three different normality ranges have been considered: ±σ, ±1.5σ and ±2σ. Patients with regional SUVr values falling outside the corresponding lower normality range were considered hypometabolic.

2.3.3. Reference analysis methods

In order to calibrate the proposed PET analysis pipeline and the normality range to best agree with reference methods in identifying hypometabolic regions, results were compared with standard analysis methods: visual analysis supported by a vendor tool and SPM statistical analysis with two different parameterizations.

Visual analysis. All patients' images were evaluated by one rater, a Nuclear Medicine specialist with more than 10 years of experience, supported in the analysis by the Cortex ID Suite (GE Healthcare). The rater was instructed to binary categorize each pre-defined ROI as hypometabolic or normal.

2.3.3.1. *Conventional SPM analysis (SPM-A) [33,34].*

- Pre-processing: after a reorientation phase, each scan was spatially normalized to MNI space through affine transformation and interpolated to a voxel grid of 2 x 2 × 2 mm^3. Normalized images were smoothed with an isotropic Gaussian kernel with FWHM = 8 mm.

- Statistical analysis: A two-sample *t*-test was performed for each patient to test for relative hypometabolism by comparing the patient as the first group (n = 1) and the reference healthy control group as the second group (n = 107). Age was considered a covariate. Cluster-level significance threshold was set at $p < 0.001$ (uncorrected). A cluster size threshold of 100 voxels was considered.

2.3.3.2. High-resolution SPM analysis (SPM-B).

- Pre-processing: pre-processing used in the proposed analysis pipeline. It differs from SPM-A in the interpolation grid (1 mm instead of 2 mm) and in the presence of PVE correction instead of smoothing.

- Statistical analysis: as in SPM-A, but with cluster-level significance threshold set at $p < 0.01$ (uncorrected), cluster size threshold set at 800 voxels.

The t-maps provided by SPM-A and SPM-B analysis were read by the AAL3 Cluster Labeling Toolbox (https://www.gin.cnrs.fr/en/tools/aal/) of SPM12, and properly customized to match the 16 ROIs used in the proposed pipeline. Significant clusters were associated with the corresponding ROIs, which were thus marked as hypometabolic.

2.3.4. Statistical analysis and quantitative tool validation

For each ROI and for each normality range, results obtained with the proposed pipeline were compared with the three reference methods in terms of accuracy, sensitivity, and specificity in properly identifying hypometabolic patients (ROI-level comparison, ROIs labeled as 1 if hypometabolic). Agreement was also statistically assessed through adjusted Cohen's κ [35], considering prevalence and balance indexes [36]. To have a reference for results evaluation, an intra-reference comparison was performed as well: SPM-A and SPM-B were both compared to visual analysis; SPM-B was compared to SPM-A, the most commonly used in the literature [33,34,37].

In order to select the normality range that would make the pipeline agreement vs reference methods in line with the intra-reference agreement, a Student's *t-test* (or non-parametric test in non-normality conditions) was run between the pipeline Cohen's κ and the reference methods Cohen's κ, assuming one of the reference methods as the standard for the Cohen's κ calculation. The normality range whose Cohen's κ belonged to the same group as the reference methods Cohen's κ was then selected (significance level was set at *p-value* < 0.05).

All Figures of Merit (FOMs) computation, i.e., accuracy, sensitivity, specificity, and Cohen's κ, and all the statistical analyses were performed using Stata^{MP} (version 17.0; Stata Corp., College Station, USA).

2.4. Preliminary joint PET-pCASL analysis on 5 MCI patients

The entire pipeline and the selected PET normality range were preliminarily applied to a group of 5 MCI patients. For each patient, SUVr and CBFr values obtained in right and left ROIs were considered separately. For each cortical region, the Pearson Correlation Coefficient (PCC) between SUVr and CBFr values was assessed.

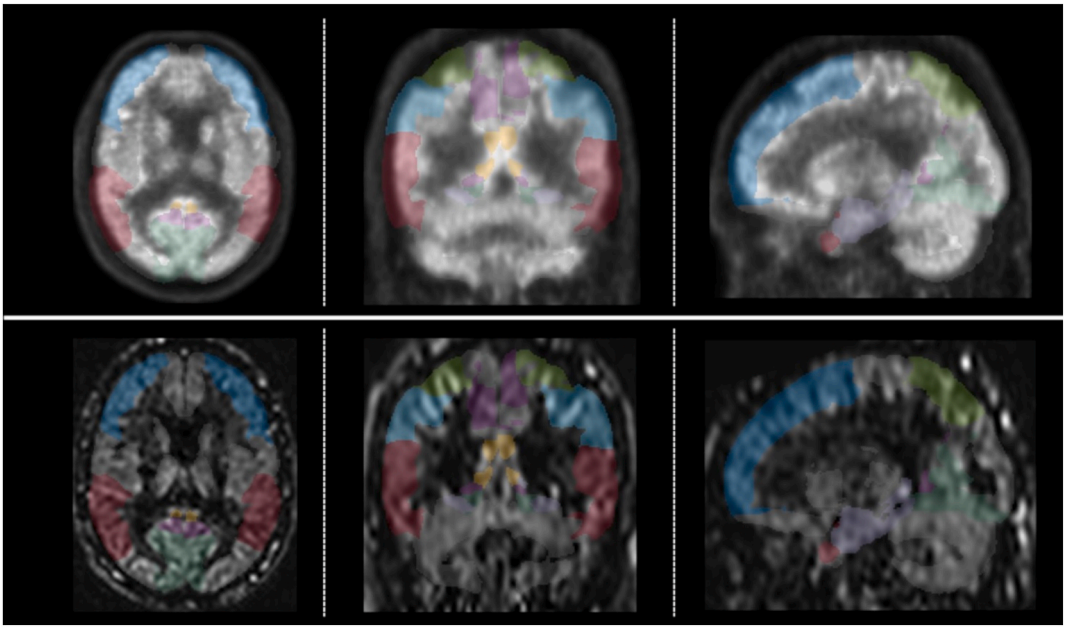

Fig. 2. Axial, coronal and sagittal view of a ^{18}F-FDG PET (upper panel) and pCASL (lower panel) normalized images with selected ROIs (left and right) superimposed. Posterior Cingulum (yellow), Occipital Cortex (dark green), Lateral Temporal Cortex (red), Mesial Temporal Cortex (lilac), Precuneus (violet), Lateral Prefrontal Cortex (blue), Inferior (cyan) and Superior Parietal Cortex (light green) are considered.

3. Results

3.1. Regions of interest (ROIs)

Fig. 2 shows the selected ROIs superimposed to a ^{18}F-FDG PET study and a pCASL study in axial, coronal, and sagittal planes. Table 1 reports ROIs volume (mL).

3.2. Proposed ROI-based quantitative analysis pipeline output

Fig. 3 reports the outcome of the ROI-based analysis pipeline on a patient example. SUVr and CBFr values for the 16 ROIs are represented with a histogram for PET and pCASL respectively; the horizontal line corresponds to the cerebellum SUV(CBF), against which SUV(CBF) ROI values are normalized. For both SUVr and CBFr histograms, corresponding left and right ROIs are mirrored and associated with the same color, to better appreciate metabolism and perfusion symmetry/asymmetry levels. For this patient, a common pattern between metabolism and perfusion can be noticed: regions with a lower metabolism than the cerebellum are generally also less perfused.

3.3. Validation and tuning of the PET line

3.3.1. ROI hypometabolism assessment with reference methods

SPM-A and SPM-B outcomes consist in t-maps of significant clusters, each one associated to local maxima coordinates in mm (Fig. 4a and c). The corresponding cluster labeling table provided by the AAL3 toolbox is shown in Fig. 4b and d.

Table 2 lists hypometabolic occurrences detected by the three reference analysis methods on the 36 patients. For each ROI, occurrences are expressed as the percentage of patients found to be hypometabolic in that region.

3.3.2. ROI hypometabolism assessment with the proposed pipeline

In Table 3, mean and standard deviation of SUVr values on the 107 healthy subjects are reported for the 16 ROIs.

Fig. 5, as an example, reports the PET line analysis results for a 68 years old MCI patient. Patient SUVr values in the 16 ROIs are shown as color bars, together with corresponding healthy patients mean SUVr values (black circles) and σ, 1.5σ, and 2σ normality ranges (black lines). For this patient, a high level of symmetry and bilateral temporo-parietal hypometabolism can be noticed, as a typical AD pattern [31]. It can be particularly appreciated how inferior parietal cortices SUVr (cyan bars) and lateral temporal cortices SUVr (red bars) are both lower than ($<2\sigma$) SUVr in healthy subjects, and therefore are categorized as hypometabolic with all the three normality ranges. Left and right superior parietal cortices SUVr (light green bars) are instead lower than ($<1.5\sigma$) and larger than ($<2\sigma$) SUVr in healthy subjects, and therefore would be classified as hypometabolic with σ and 1.5σ normality range and as normal with the 2σ normality range.

3.3.3. Agreement with reference analysis methods and normality range selection

Agreement with reference methods and intra-reference methods are shown in Table 4, in terms of mean and standard deviation over the 16 ROIs of accuracy, sensitivity, specificity, and adjusted Cohen's κ in properly identifying hypometabolic patients. For each comparison, assessed methods are listed in rows, and reference methods in columns.

By using visual analysis as a reference, the pipeline with (σ, 1.5σ, 2σ) normality ranges obtained, on average on the 16 ROIs, accuracy (76, 78, 76)%, sensitivity (84, 67, 47)%, specificity (69, 85, 94)%, and Cohen's κ (49, 60, 60)%, respectively. With SPM-A as a reference, accuracy (71, 79, 83)%, sensitivity (89, 75, 59)%, specificity (63, 80, 93)%, and κ (42, 58, 67)% were obtained. With SPB-B as reference, accuracy (76, 77, 73)%, sensitivity (79, 64, 46)%, specificity (71, 88, 97)%, and κ (51, 54, 47)% were obtained. SPM-A (SPM-B) compared to visual analysis obtained 79 (75)% accuracy, 60 (76)% sensitivity, 92 (75)% specificity, 57 (51)% κ. SPM-B compared to SPM-A obtained 79 % accuracy, 94 % sensitivity, 72 % specificity, 58 % κ.

Results of the Student's *t-test* comparing Cohen's κ are shown in Table 5. As in Table 4, each column corresponds to a reference method assumed as the standard for the Cohen's k agreement calculation; each row reports the results of the statistical comparison between the Cohen's κ of two methods (e.g. pipeline with 1.5σ normality range and SPM-A) vs the standard.

The proposed region-based analysis pipeline with the 1.5σ normality range showed a moderate agreement [35] with reference

Table 1
ROIs volume, averaged on the left and right hemisphere.

Region	V [ml]
Posterior cingulum	2.45
Occipital Cortex	41.99
Inferior Parietal Cortex	36.87
Superior Parietal Cortex	17.21
Precuneus	25.31
Lateral Prefrontal Cortex	93.55
Lateral Temporal Cortex	92.64
Mesial Temporal Cortex	16.94

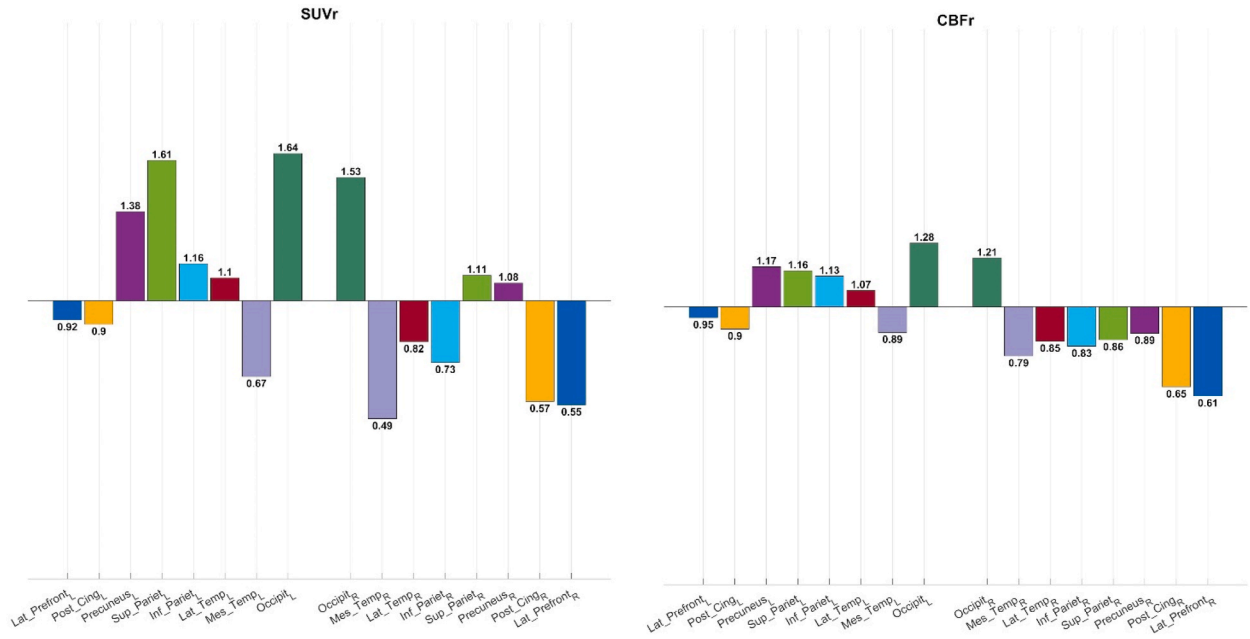

Fig. 3. For a patient's example, the histograms report SUVr (left, Fig. 3A) and CBFr (right, Fig. 3B) values in the 16 considered ROIs. Values are normalized on the cerebellar SUV (CBF) (horizontal line). Corresponding left hemisphere and right hemisphere ROIs are shown specularly and with the same color.

methods, in line with intra-reference methods agreement levels. It was therefore selected for the following evaluations.

In order to go into details of agreement levels with reference methods for the chosen 1.5σ normality range, Table 6 reports the assessed FOMs separately for each cortical region, averaged on corresponding left and right ROIs. The agreement between SPM-B and visual analysis is also reported, since SPM-B shares pre-processing with the proposed pipeline and substantially agrees with conventional SPM-A.

3.4. Preliminary joint PET-pCASL results on 5 MCI patients

For each cortical ROI, SUVr versus CBFr values patients are represented for all the 5 MCI patients in Fig. 6. ROIs identified as hypometabolic by the tuned PET line are represented with asterisks, while ROIs identified as metabolically normal are identified with circles. Regression lines and PCCs between SUVr and CBFr values are also represented.

4. Discussion

The recently proposed MR pCASL sequence is able to provide brain perfusion maps without contrast media requirement. Many groups are working to assess pCASL added value with respect to the widely used ^{18}F-FDG PET in neurodegenerative dementias. Hypometabolic areas in ^{18}F-FDG PET are clinically detected by visual analysis or with quantitative analysis tools comparing patient images with a database of healthy subjects. Healthy subject datasets for pCASL are not yet available, nor are image analysis guidelines, since sequence parameters have not been standardized yet. In this work, we propose a ROI-based analysis pipeline to quantify perfusion and metabolism in matching cortical areas on patients studied with pCASL and ^{18}F-FDG PET. Heterogeneous PET profiles of hypometabolism in different areas in MCI patients have been shown to predict progression into specific dementia subtypes [31]. The PET line is tuned and validated to identify hypometabolic regions in agreement with reference PET analysis methods. The idea is to provide a tool to compare perfusion and metabolism in hypometabolic and normo-metabolic areas in groups of patients to better understand MR pCASL and ^{18}F-FDG PET roles and synergy in MCI.

The pipeline, running on SPM12 defines steps and parameters for image preprocessing (MNI normalization, image quality enhancement, cortex segmentation) and provides average perfusion/metabolism values in 16 AAL3 cortical areas normalized to cerebellum values. Adopted choices are generally in line with similar works in literature [5,6,9,16]. pCASL and ^{18}F-FDG PET scarce image quality is properly considered.

Both methods are affected by partial volume effect (PVE), due to blurring and mixing of tissue-specific signals due to voxel heterogeneity. As to PET, PVE smooths images so that part of the radioactivity is misattributed among adjacent regions of higher and lower FDG uptake [38]. The PVE issue in PET has been addressed by several algorithms over the years, that use two (brain and non-brain) or three (gray matter, white matter, and cerebrospinal fluid) components to estimate and correct spill-in and spill-over effect [23,38–44]. In this work, we used the Müller-Gärtner method implemented in the petpve12 SPM toolbox. We preferred this

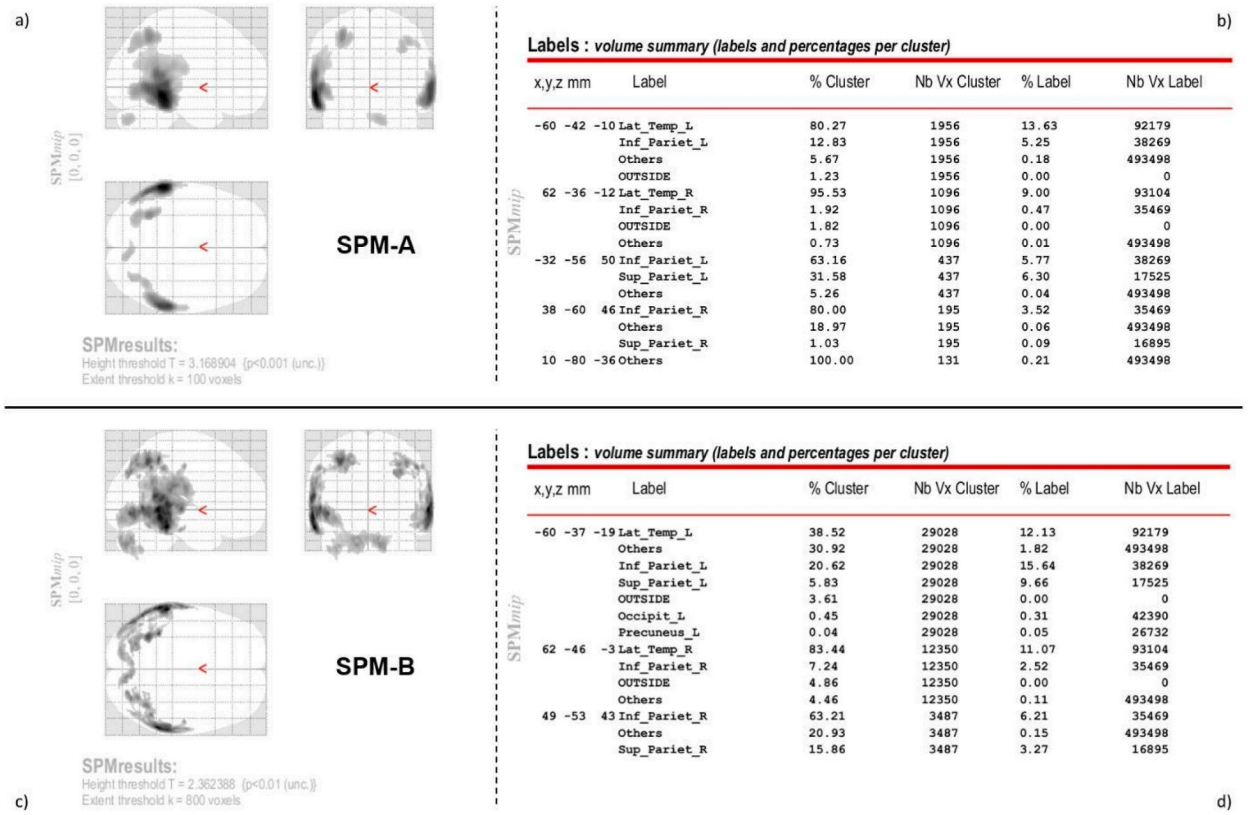

Fig. 4. Upper panel reports t-maps (a) and cluster labeling outcome (b) for SPM-A, voxel size 2x2x2 mm^3; k = 100 voxels: minimum cluster dimension to be considered as significant; $p < 0.001$ uncorrected. Lower panel reports t-maps (c) and cluster labeling outcome (d) for SPM-B, voxel size 1x1x1 mm^3; k = 800 voxels: minimum cluster dimension to be considered as significant ($p < 0.01$ uncorrected at voxel-level). All significant clusters, identified by a local maxima given in millimeters coordinates, are associated to regions listed in "Labels" tables (b,d) in specific percentages.

Table 2
Hypometabolic occurrences [%], identified by the three reference analysis methods on the 36 patients.

	Visual analysis – Cortex	SPM-A	SPM-B
Left Posterior cingulum	0.42	0.11	0.28
Right Posterior cingulum	0.39	0.08	0.22
Left Occipital Cortex	0.19	0.17	0.47
Right Occipital Cortex	0.17	0.17	0.33
Left Inferior Parietal Cortex	0.61	0.47	0.58
Right Inferior Parietal Cortex	0.44	0.36	0.58
Left Superior Parietal Cortex	0.39	0.22	0.44
Right Superior Parietal Cortex	0.36	0.25	0.42
Left Precuneus	0.56	0.25	0.50
Right Precuneus	0.47	0.25	0.42
Left Lateral Prefrontal Cortex	0.47	0.31	0.53
Right Lateral Prefrontal Cortex	0.36	0.33	0.56
Left Lateral Temporal Cortex	0.67	0.64	0.78
Right Lateral Temporal Cortex	0.39	0.53	0.67
Left Mesial Temporal Cortex	0.42	0.36	0.36
Right Mesial Temporal Cortex	0.39	0.28	0.39

approach rather than Rousset's GTM since GTM requires an a priori GM parcellation scheme and assumes a homogenous tracer signal within the parcellated GM structures, that may not hold true for all the considered ROIs [24]. Anyhow, a comparison between MG and Symmetric Geometric Transfer Matrix method (SGTM), which is similar to GTM in terms of accuracy [45], showed no significant difference in assessing mean uptake values in ROI-based analysis [46]. The signal cross-contamination issue in pCASL is more challenging [21]. In the last decades some studies have developed algorithms for PVE correction in arterial spin labelling [21,42,47,48], but the employed methodologies still remain inconsistent and no consensus has emerged on the best method to use [49]. Therefore, a

Table 3
Mean and standard deviation (σ, in brackets) of SUVr values for each of the 16 ROIs on the 107 healthy subjects are reported.

Region	Left hemisphere	Right hemisphere
Posterior cingulum	1.54 (0.27)	1.46 (0.29)
Occipital Cortex	1.46 (0.16)	1.39 (0.16)
Inferior Parietal Cortex	1.24 (0.19)	1.34 (0.21)
Superior Parietal Cortex	1.24 (0.30)	1.21 (0.30)
Precuneus	1.45 (0.17)	1.48 (0.16)
Lateral Prefrontal Cortex	1.33 (0.21)	1.41 (0.23)
Lateral Temporal Cortex	1.16 (0.12)	1.21 (0.13)
Mesial Temporal Cortex	0.73 (0.07)	0.74 (0.07)

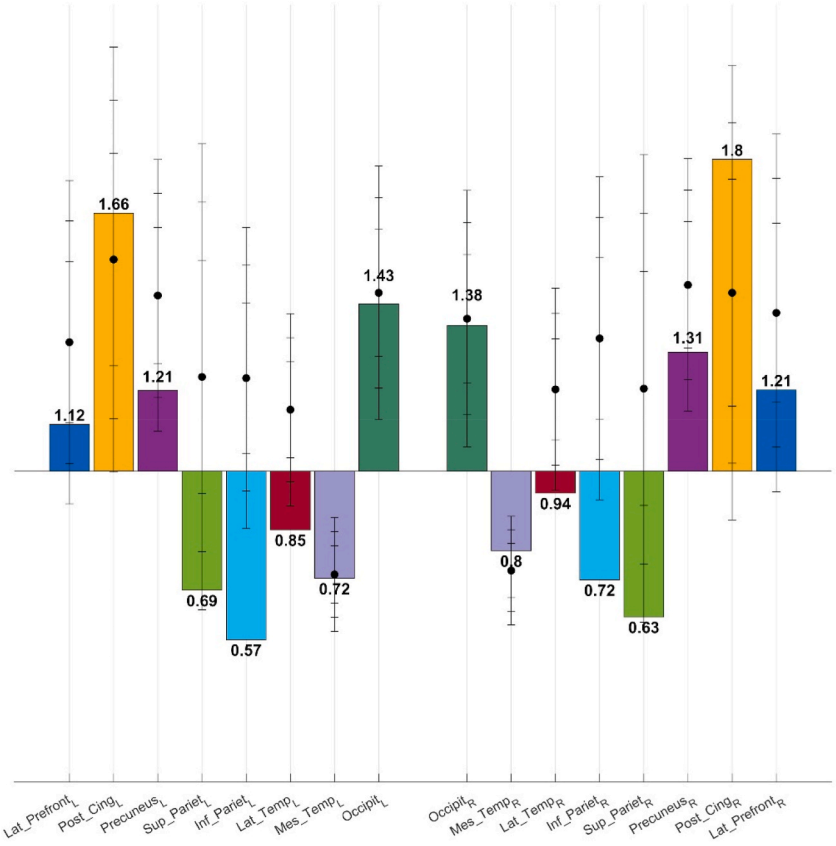

Fig. 5. SUVr in the 16 ROIs for an example MCI patient (colored bars) with superimposed normative data, i.e. mean SUVr values (black circles) and σ, 1.5σ, and 2σ normality ranges (black lines) computed on the 107 healthy patients.

more conventional and diffuse spatial smoothing was chosen to improve pCASL quality after MNI normalization. A coherent FWHM = 6 mm was applied to both PET and pCASL to match final spatial resolutions [16]. When a consensus about the best methodology to use will be available in literature, we will accordingly improve the analysis pipeline.

As to GM segmentation, a mean TPM was used instead of patient-specific structural images. This choice was motivated by the necessity to coherently process patient and PET healthy subjects, that are devoid of structural images. Although it has been shown in literature that a mean GM could allow better inter- and intra-subject correspondence [50,51], we are aware of the possible sub-optimality of this choice. On a small group of 5 MCI patients, we compared CBFr values obtained with GM segmentations derived from TPM and from patient-specific T1 images (data not shown), and we observed a mean and maximum percentage variation of 4 % and 10 %, respectively. The TPM-based GM segmentation appears therefore not excessively affecting pCASL mean CBFr values in ROIs. When normative PET data with T1 images will become available, we will improve the pipeline to exploit T1 for the GM definition.

Other ASL analysis tools are available for the community, like the ExploreASL toolbox [52] that is completely dedicated to ASL processing and analysis, and includes PVE correction as well. However, since our aim was to coherently analyze PET and pCASL images, we decided to use the SPM toolbox for both images. In future developments, we intend to compare results obtained with the

Table 4
Mean (standard deviation, SD) of Accuracy (%), Sensitivity (%), Specificity (%) and adjusted Cohen's κ, obtained as average on all the 16 ROIs parameters respectively. Each parameter is defined by assessing the considered analysis method listed in rows with respect to the three reference methods listed in columns. Cohen's K are given with CI = 95 %.

	Visual analysis - Cortex				SPM-A				SPM-B			
	Accuracy	Sensitivity	Specificity	Cohen's κ	Accuracy	Sensitivity	Specificity	Cohen's κ	Accuracy	Sensitivity	Specificity	Cohen's κ
σ	0.76 (0.08)	0.84 (0.12)	0.69 (0.10)	0.49 (0.17)	0.71 (0.07)	0.89 (0.12)	0.63 (0.10)	0.42 (0.14)	0.76 (0.09)	0.79 (0.17)	0.71 (0.11)	0.51 (0.18)
1.5 σ	0.78 (0.08)	0.67 (0.14)	0.85 (0.10)	0.60 (0.17)	0.79 (0.06)	0.75 (0.19)	0.80 (0.08)	0.58 (0.12)	0.77 (0.10)	0.64 (0.18)	0.88 (0.12)	0.54 (0.20)
2 σ	0.76 (0.08)	0.47 (0.18)	0.94 (0.05)	0.60 (0.21)	0.83 (0.06)	0.59 (0.19)	0.93 (0.05)	0.67 (0.13)	0.73 (0.09)	0.46 (0.17)	0.97 (0.05)	0.47 (0.19)
SPM-B	0.75 (0.08)	0.76 (0.14)	0.75 (0.14)	0.51 (0.15)	0.79 (0.05)	0.94 (0.08)	0.72 (0.10)	0.58 (0.11)				
SPM-A	0.79 (0.07)	0.60 (0.20)	0.92 (0.07)	0.57 (0.15)								

Table 5
Student's *t-tests* results (non-parametric Wilcoxon sign rank test in non-normality conditions) for Cohen's κ outcomes. Tests were applied for groups that are coupled and listed in rows. Each column refers to the methods considered as reference in Cohen's κ calculation. H0: same level of agreement with respect to the method in column. The *p-value* was set at $p < 0.05$.

	Visual analysis - Cortex	SPM-A
σ vs SPM-A	0.172	
1.5 σ vs SPM-A	0.616	
2 σ vs SPM-A	0.051	
σ vs SPM-B	0.943	0.006*
1.5 σ vs SPM-B	0.312	1.000
2 σ vs SPM-B	0.954	0.040*

Table 6
Mean (standard deviation, SD) of Accuracy (%), Sensitivity (%), Specificity (%) and adjusted Cohen's κ as average of left and right side of each selected ROI given.

	Accuracy	Sensitivity	Specificity	Cohen's κ
1.5 σ vs **Visual analysis - Cortex**				
Posterior cingulum	0.69 (0.00)	0.41 (0.02)	0.88 (0.03)	0.39 (0.00)
Occipital Cortex	0.90 (0.02)	0.61 (0.15)	0.97 (0.00)	0.81 (0.04)
Inferior Parietal Cortex	0.78 (0.08)	0.76 (0.02)	0.81 (0.16)	0.56 (0.16)
Superior Parietal Cortex	0.76 (0.02)	0.70 (0.02)	0.80 (0.03)	0.53 (0.04)
Precuneus	0.72 (0.08)	0.62 (0.04)	0.84 (0.14)	0.44 (0.16)
Lateral Prefrontal Cortex	0.76 (0.14)	0.68 (0.20)	0.82 (0.11)	0.53 (0.27)
Lateral Temporal Cortex	0.85 (0.02)	0.82 (0.05)	0.91 (0.13)	0.69 (0.04)
Mesial Temporal Cortex	0.75 (0.04)	0.73 (0.08)	0.77 (0.01)	0.50 (0.08)
1.5 σ vs **SPM-A**				
Posterior cingulum	0.78 (0.08)	0.54 (0.29)	0.80 (0.06)	0.56 (0.16)
Occipital Cortex	0.86 (0.04)	0.50 (0.24)	0.93 (0.00)	0.72 (0.08)
Inferior Parietal Cortex	0.81 (0.08)	0.86 (0.03)	0.77 (0.10)	0.61 (0.16)
Superior Parietal Cortex	0.79 (0.02)	0.88 (0.01)	0.76 (0.02)	0.58 (0.04)
Precuneus	0.82 (0.06)	0.64 (0.08)	0.78 (0.05)	0.64 (0.12)
Lateral Prefrontal Cortex	0.78 (0.04)	0.78 (0.05)	0.78 (0.08)	0.56 (0.08)
Lateral Temporal Cortex	0.79 (0.02)	0.74 (0.00)	0.86 (0.03)	0.58 (0.04)
Mesial Temporal Cortex	0.69 (0.04)	0.71 (0.13)	0.69 (0.00)	0.39 (0.08)
1.5 σ vs **SPM-B**				
Posterior cingulum	0.79 (0.06)	0.55 (0.07)	0.87 (0.07)	0.58 (0.12)
Occipital Cortex	0.68 (0.06)	0.27 (0.03)	0.95 (0.01)	0.36 (0.12)
Inferior Parietal Cortex	0.81 (0.16)	0.76 (0.13)	0.87 (0.18)	0.61 (0.31)
Superior Parietal Cortex	0.93 (0.02)	0.87 (0.01)	0.98 (0.03)	0.86 (0.04)
Precuneus	0.81 (0.04)	0.73 (0.01)	0.88 (0.10)	0.61 (0.08)
Lateral Prefrontal Cortex	0.81 (0.00)	0.69 (0.06)	0.94 (0.08)	0.61 (0.00)
Lateral Temporal Cortex	0.68 (0.10)	0.61 (0.10)	0.88 (0.18)	0.36 (0.20)
Mesial Temporal Cortex	0.67 (0.02)	0.63 (0.02)	0.69 (0.01)	0.33 (0.00)
SPM-B vs Visual analysis - Cortex				
Posterior cingulum	0.76 (0.02)	0.52 (0.02)	0.93 (0.04)	0.53 (0.04)
Occipital Cortex	0.69 (0.04)	0.76 (0.13)	0.68 (0.08)	0.39 (0.08)
Inferior Parietal Cortex	0.75 (0.16)	0.81 (0.08)	0.70 (0.22)	0.50 (0.31)
Superior Parietal Cortex	0.81 (0.04)	0.81 (0.06)	0.80 (0.03)	0.61 (0.08)
Precuneus	0.75 (0.04)	0.70 (0.07)	0.80 (0.02)	0.50 (0.08)
Lateral Prefrontal Cortex	0.71 (0.18)	0.79 (0.13)	0.66 (0.19)	0.42 (0.35)
Lateral Temporal Cortex	0.78 (0.08)	0.98 (0.03)	0.56 (0.03)	0.56 (0.16)
Mesial Temporal Cortex	0.78 (0.00)	0.69 (0.03)	0.84 (0.03)	0.56 (0.00)

proposed pipeline with those provided by ExploreASL.

As to the choice of reference PET analysis methods for normality range definition, EANM guidelines for brain PET imaging admit the use of both visual and software-aided approaches, recommending their combined use. A preferred method has not been clearly indicated yet. Several studies have evaluated the added value of semiautomatic tools in the clinical setting and showed a higher specificity compared with visual reading, especially (but not only) for the identification of AD-related patterns, thereby increasing diagnostic confidence [30,33,53–55]. Other studies reported a similar sensitivity, although visual analysis is obviously affected by the reader experience [30,56,57]. For this reason, we decided to consider both visual analyses supported by software already used in clinics (Cortex ID), and the popular SPM analysis as reference methodologies for the assessment of hypometabolic cortical areas on ^{18}F-FDG PET images. A consideration needs to be made about the comparison with SPM. SPM provides a voxel-wise analysis, i.e.

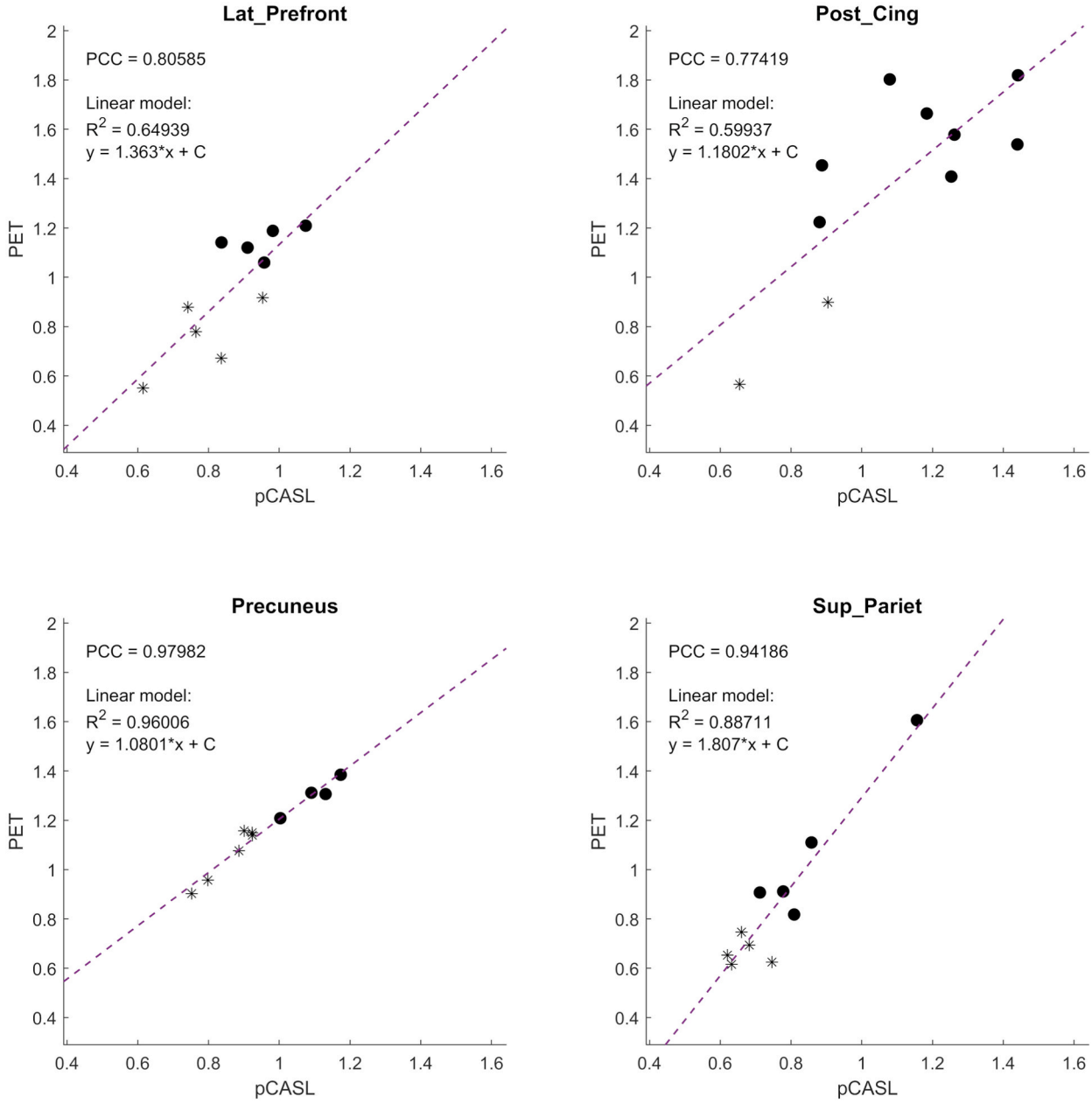

Fig. 6. Scatter plots of CBFr versus SUVr values are shown for each ROI (above, Fig. 6A: Lateral Prefrontal Cortex, Posterior Cingulum, Precuneus, Superior Parietal Cortex; below, Fig. 6B: Inferior Parietal Cortex, Lateral Temporal Cortex, Mesial Temporal Cortex, Occipital Cortex). Five MCI patients are reported and values of right and left hemisphere are drawn separately. A regression line is superimposed and Pearson's Correlation Coefficients (PCC) are reported. Regression model characteristics are also depicted in each ROI caption as $y = \beta_1 x + C$ (where only β_1 are expressed specifically for each regression). ROIs identified as hypometabolic by the tuned PET line are represented with asterisks.

hypometabolic areas are defined as clusters of voxels that are significantly different from the healthy control group. Those clusters may not necessarily correspond to the macro regions chosen for the proposed ROI-based analysis. They could result as portions of those ROIs or could be associated with more than one ROI. To overcome the inherent limit in comparing SPM voxel wise analysis and ROI-based analysis, the AAL3 Cluster Labeling Toolbox was used.

The SPM parametrization here identified as SPM-A is considered a standard in the literature, robust towards both PET scanner models and differences in healthy control groups, and therefore reliable for longitudinal and multicenter studies [58]. The higher resolution SPM-B parametrization was also considered, with the specific aim of assessing the impact of a smaller voxel size, fitting with MRI spatial resolution, and a different image quality enhancement.

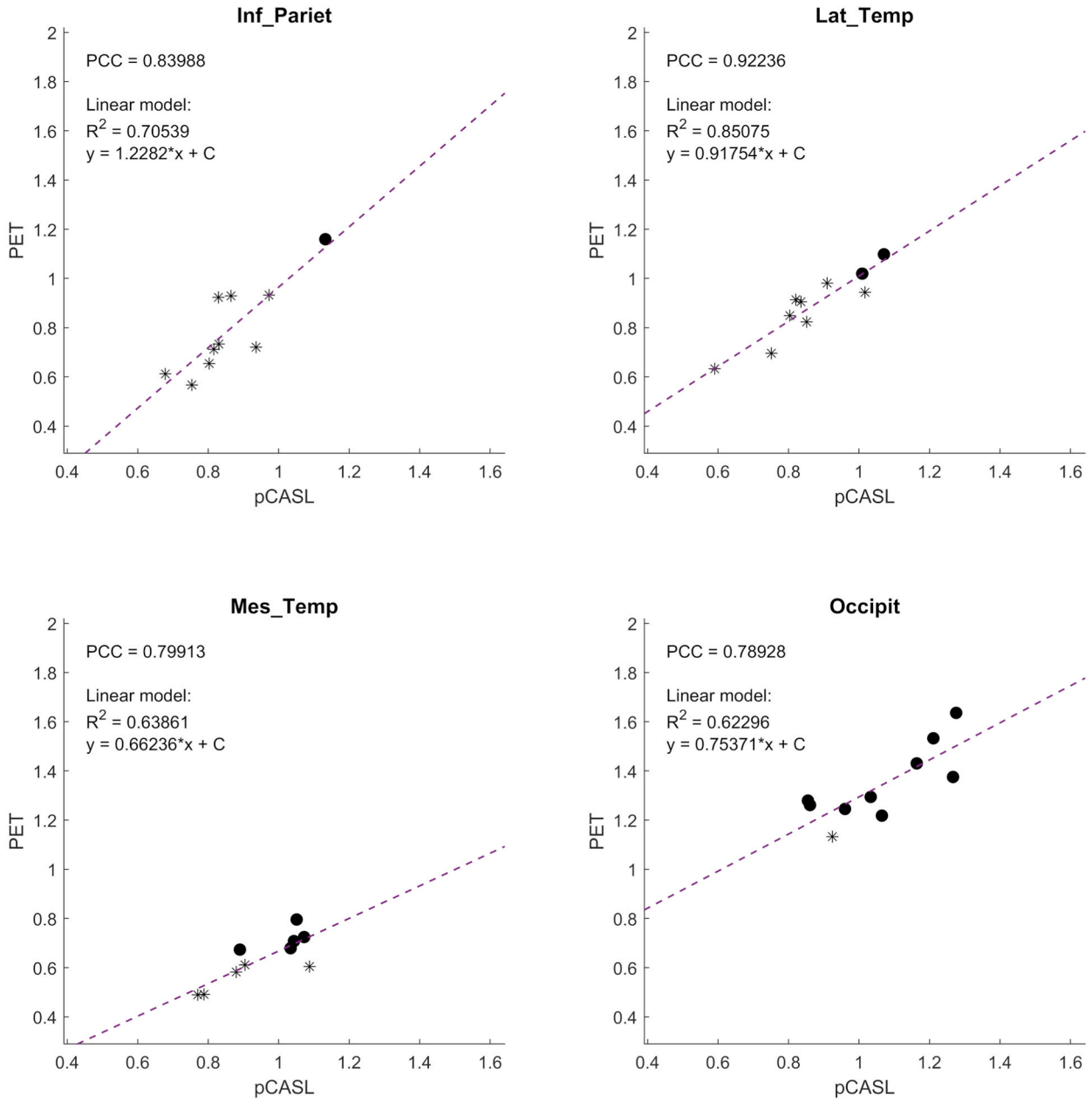

Fig. 6. (*continued*).

Differences between the three reference methods are expected [30,56,59,60] and can be observed in Table 2. Across almost all cortical ROIs, SPM-B is the strategy that identifies more patients as hypometabolic. SPM with a 1 x 1 × 1 mm^3 voxel grid has been previously used on digital PET images, showing a higher sensitivity in discriminating AD using health control acquired on digital scanners rather than using conventional controls [60]. Furthermore, visual analysis shows a higher incidence of hypometabolic regions with respect to SPM-A, in accordance with previously published studies [30,56] that showed how a trained reader can pick up subtle abnormalities that do not reach the threshold of statistical significance, probably due to his ability to highlight inter-hemispheric asymmetries in critical areas, a feature that is not available in the Z scoring system or in SPM. On average, on the 16 considered ROIs, SPM-A and SPM-B, if compared with visual analysis supported by Cortex ID, obtained an accuracy of 79 % and 75 %, a sensitivity of 60 % and 76 %, a specificity of 92 % and 75 %, and a Cohen's κ of 57 % and 51 %, respectively. SPM-B if compared with SPM-A showed a higher incidence of hypometabolic regions and obtained an accuracy of 79 % and a Cohen's κ of 58 %.

The SUVr normality range for the proposed pipeline was selected in order to obtain an agreement vs reference methods statistically comparable with intra-reference methods agreement. The 1.5σ normality range was chosen as it generally has the highest accuracy and Cohen's κ with respect to reference methods, providing agreement values that are in line with intra-reference methods agreement

levels: accuracy of 78 % and Cohen's κ 60 % vs visual analysis, accuracy of 79 % and Cohen's κ 58 % vs SPM-A, accuracy of 77 % and Cohen's κ 54 % vs SPM-B. Furthermore, Cohen's κ is not significantly different from SPM-A and SPM-B Cohen's κ when assuming visual analysis as reference method (*p-value* 0.61 and 0.31 respectively). Considering SPM-A as reference method, Cohen's κ is not significantly different from SPM-B Cohen's κ as well (*p-value* = 1.00).

The 2σ normality range has the highest agreement with SPM-A in terms of accuracy (83 %), specificity (93 %) and Cohen's κ (67 %), but the sensitivity is unacceptably low (59 %). Furthermore, the Cohen's κ vs SPM-A significantly differs from SPM-B Cohen's κ vs the same reference (*p-value* 0.04). The 1σ normality range, conversely, shows high sensitivity, but other FOMs have the lowest values in almost all the comparisons. The Cohen's κ vs SPM-A significantly differs from SPM-B Cohen's κ vs the same reference (*p-value* 0.0065). Different thresholds in the normality range definition would lead to improved sensitivity or specificity in hypometabolic areas detection and therefore could be considered clinically preferable in some contexts. However, this type of evaluation is beyond the scope of this work.

Focusing on the 1.5σ normality range and on results obtained on different cortical regions (Table 6), we can appreciate that, except for the Posterior Cingulum and Precuneus in the comparison with visual analysis and for the mesial temporal cortex in the comparison with SPM-A, accuracies larger than 75 %, and Cohen's κ larger than 50 % are always obtained. In the comparison with SPM-B, accuracies lower than 70 %, and Cohen's κ lower than 50 % are obtained only in the occipital cortex, lateral temporal cortex, and mesial temporal cortex.

In the last part of the work, we preliminary applied the proposed pipeline and the associated PET normality range to a group of 5 MCI patients. Despite the small sample, we can observe how hypometabolic areas are generally also hypoperfused and how these are the typical regions affected in prodromal AD, such as temporo-parietal, precuneus and posterior cingulate cortex.

The PCC values in ROIs are in line with or even higher than those found in similar studies on Alzheimer's or healthy populations. For example, Yan et al. defined 9 ROIs starting from the Automated Anatomical Labeling Atlas in SPM and calculating PCC for each ROI. They obtained PCC = 0.34 in occipital cortex and PCC = 0.22 in temporal cortex [6].

A previous study comparing ASL-MRI and FDG-PET in MCI patients demonstrated that patterns and strength of hypoperfusion and hypometabolism in MCI were comparable [13], but they used different reference regions for each technique. Our proposed method answers to the need for more automated approaches with respect to visual analysis, providing CBFr and SUVr in the same regions. Thus, it could add more information about the deviation from the PET normality range.

In conclusion, a SPM12-based analysis pipeline combining ^{18}F-FDG PET and pCASL imaging in MCI patients was presented. The PET line, exploiting the availability of a large database of healthy subjects, has been tuned in order to individuate hypometabolic ROIs in agreement with reference methods used in nuclear medicine clinics. The full PET-pCASL pipeline has been preliminary applied to a group of 5 MCI patients, where it has shown high correlations between metabolism and perfusion, in particular in known regions of early AD neurodegeneration. The proposed approach appears reliable to be further applied in PET-pCASL MCI studies, even in the absence of a pCASL healthy group, to assess relative correlation between/within selected regions, and between/within the two modalities. Future perspectives for this approach could also be its validation in longitudinal studies, where its predictive value for disease progression could be evaluated. This will help to better define if pCASL can provide a reasonable alternative for FDG-PET in this scenario.

Funding

This research did not receive any specific grant from funding agencies in the public, commercial, or not-for-profit sectors.

Ethics statement

Ethics approval number: 3974 (May 05, 2022), Comitato Etico Brianza.

CRediT authorship contribution statement

Valeria Cerina: Conceptualization, Data curation, Formal analysis, Methodology, Software, Validation, Visualization, Writing – original draft, Writing – review & editing. **Cinzia Crivellaro:** Conceptualization, Investigation, Resources, Writing – original draft, Writing – review & editing. **Sabrina Morzenti:** Conceptualization, Investigation, Supervision, Writing – review & editing. **Federico E. Pozzi:** Conceptualization, Investigation, Resources, Writing – review & editing. **Vittorio Bigiogera:** Investigation. **Lorenzo Jonghi-Lavarini:** Investigation. **Rosa M. Moresco:** Supervision, Writing – review & editing. **Gianpaolo Basso:** Conceptualization, Investigation, Project administration, Resources, Supervision. **Elisabetta De Bernardi:** Conceptualization, Methodology, Project administration, Supervision, Visualization, Writing – original draft, Writing – review & editing.

Declaration of competing interest

The authors declare that they have no known competing financial interests or personal relationships that could have appeared to influence the work reported in this paper.

References

[1] M. Boccardi, et al., Italian consensus recommendations for a biomarker-based aetiological diagnosis in mild cognitive impairment patients, Eur. J. Neurol. 27 (3) (Mar. 2020) 475–483, https://doi.org/10.1111/ENE.14117.

[2] C. Festari, et al., European consensus for the diagnosis of MCI and mild dementia: Preparatory phase, Alzheimer's Dementia 19 (5) (2022) 1729–1741, https://doi.org/10.1002/ALZ.12798.

[3] S. Haller, G. Zaharchuk, D.L. Thomas, K.-O. Lovblad, F. Barkhof, X. Golay, Arterial spin labeling perfusion of the brain, Radiology 281 (2) (2016) 337–356, https://doi.org/10.1148/radiol.2016150789.

[4] D.C. Alsop, et al., Recommended Implementation of arterial spin-labeled perfusion MRI for clinical applications: a consensus of the ISMRM perfusion study group and the European consortium for ASL in dementia 73 (1) (2015) 102–116, https://doi.org/10.1002/mrm.25197.

[5] Y.H.K. Cha, M.A. Jog, Y.C. Kim, S. Chakrapani, S.M. Kraman, D.J.J. Wang, Regional correlation between resting state FDG PET and pCASL perfusion MRI, J. Cerebr. Blood Flow Metabol. 33 (12) (2013), https://doi.org/10.1038/JCBFM.2013.147, 1909–1914, Dec.

[6] L. Yan, et al., Regional association of pCASL-MRI with FDG-PET and PiB-PET in people at risk for autosomal dominant Alzheimer's disease, NeuroImage Clin 17 (2018) 751–760, https://doi.org/10.1016/j.nicl.2017.12.003, 2017.

[7] Y. Chen, et al., Voxel-level comparison of arterial spin-labeled perfusion MRI and FDG-PET in Alzheimer disease, Neurology 77 (22) (Nov. 2011), https://doi.org/10.1212/WNL.0B013E31823A0EF7, 1977–1985.

[8] E.S. Musiek, et al., Direct comparison of fluorodeoxyglucose positron emission tomography and arterial spin labeling magnetic resonance imaging in Alzheimer's disease, Alzheimer's Dementia 8 (1) (Jan. 2012) 51–59, https://doi.org/10.1016/J.JALZ.2011.06.003.

[9] S.C.J. Verfaillie, et al., Cerebral perfusion and glucose metabolism in Alzheimer's disease and frontotemporal dementia: two sides of the same coin? Eur. Radiol. 25 (10) (Oct. 2015) 3050–3059, https://doi.org/10.1007/S00330-015-3696-1.

[10] D. Tosun, et al., Diagnostic utility of ASL-MRI and FDG-PET in the behavioral variant of FTD and AD, Ann. Clin. Transl. Neurol. 3 (10) (2016) 740–751, https://doi.org/10.1002/acn3.330.

[11] D. Tosun, N. Schuff, W. Jagust, M.W. Weiner, Discriminative power of arterial spin labeling magnetic resonance imaging and 18F-fluorodeoxyglucose positron emission tomography changes for amyloid-β-positive subjects in the Alzheimer's disease continuum, Neurodegener. Dis. 16 (1–2) (2016) 87–94, https://doi.org/10.1159/000439257.

[12] I. Riederer, et al., Alzheimer disease and mild cognitive impairment: integrated pulsed arterial spin-labeling MRI and18F-FDG PET, Radiology 288 (1) (2018) 198–206, https://doi.org/10.1148/radiol.2018170575.

[13] S. Dolui, Z. Li, I.M. Nasrallah, J.A. Detre, D.A. Wolk, Arterial spin labeling versus 18F-FDG-PET to identify mild cognitive impairment, NeuroImage Clin 25 (Jan. 2020) 102–146, https://doi.org/10.1016/J.NICL.2019.102146.

[14] S. Verclytte, et al., Cerebral hypoperfusion and hypometabolism detected by arterial spin labeling MRI and FDG-PET in early-onset alzheimer's disease, J. Neuroimaging 26 (2) (Mar. 2015) 207–212, https://doi.org/10.1111/JON.12264.

[15] J. Wang, et al., The relationship among glucose metabolism, cerebral blood flow, and functional activity: a hybrid PET/fMRI study, Mol. Neurobiol. 58 (6) (Jun. 2021) 2862–2873, https://doi.org/10.1007/S12035-021-02305-0.

[16] U.C. Anazodo, et al., Using simultaneous PET/MRI to compare the accuracy of diagnosing frontotemporal dementia by arterial spin labelling MRI and FDG-PET, NeuroImage. Clin. 17 (2017) 405–414, https://doi.org/10.1016/J.NICL.2017.10.033.

[17] P. Clement, et al., ASL-BIDS, the brain imaging data structure extension for arterial spin labeling, Sci. Data 9 (1) (2022) 543, https://doi.org/10.1038/s41597-022-01615-9.

[18] M.S. Albert, et al., The diagnosis of mild cognitive impairment due to Alzheimer's disease: recommendations from the National Institute on Aging-Alzheimer's Association workgroups on diagnostic guidelines for Alzheimer's disease, Alzheimer's Dementia 7 (3) (2011) 270–279, https://doi.org/10.1016/j.jalz.2011.03.008.

[19] R.C. Petersen, B. Caracciolo, C. Brayne, S. Gauthier, V. Jelic, L. Fratiglioni, Mild cognitive impairment: a concept in evolution, J. Intern. Med. 275 (3) (2014) 214–228, https://doi.org/10.1111/joim.12190.

[20] E. Guedj, et al., EANM procedure guidelines for brain PET imaging using [18F]FDG, version 3, Eur. J. Nucl. Med. Mol. Imaging 49 (2) (Jan. 2022) 632–651, https://doi.org/10.1007/S00259-021-05603-W.

[21] I. Asllani, A. Borogovac, T.R. Brown, Regression algorithm correcting for partial volume effects in arterial spin labeling MRI, Magn. Reson. Med. 60 (6) (2008) 1362–1371, https://doi.org/10.1002/mrm.21670.

[22] P. Clement, et al., A beginner's guide to arterial spin labeling (ASL) image processing, Front. Radiol. 2 (Jun. 2022), https://doi.org/10.3389/FRADI.2022.929533, 929–533.

[23] H.W. Müller-Gärtner, et al., Measurement of radiotracer concentration in brain gray matter using positron emission tomography: MRI-based correction for partial volume effects, J. Cerebr. Blood Flow Metabol. 12 (4) (1992) 571–583, https://doi.org/10.1038/jcbfm.1992.81. Jul.

[24] G. Gonzalez-Escamilla, C. Lange, S. Teipel, R. Buchert, M.J. Grothe, PETPVE12: an SPM toolbox for Partial Volume Effects correction in brain PET – application to amyloid imaging with AV45-PET, Neuroimage 147 (Feb. 2017) 669–677, https://doi.org/10.1016/J.NEUROIMAGE.2016.12.077.

[25] H. Lemaître, F. Crivello, B. Grassiot, A. Alpérovitch, C. Tzourio, B. Mazoyer, Age- and sex-related effects on the neuroanatomy of healthy elderly, Neuroimage 26 (3) (Jul. 2005), https://doi.org/10.1016/J.NEUROIMAGE.2005.02.042, 900–911.

[26] B. Foster, U. Bagci, A. Mansoor, Z. Xu, D.J. Mollura, A review on segmentation of positron emission tomography images, Comput. Biol. Med. 50 (2014) 76–96, https://doi.org/10.1016/J.COMPBIOMED.2014.04.014. Jul.

[27] G.D. Kolingerid, et al., Amyloid burden quantification depends on PET and MR image processing methodology, PLoS One 16 (3) (2021), https://doi.org/10.1371/journal.pone.0248122.

[28] V. Berti, L. Mosconi, A. Pupi, Brain: normal variations and benign findings in FDG PET/CT imaging, Pet. Clin. 9 (2) (2014) 129–140, https://doi.org/10.1016/j.cpet.2013.10.006.

[29] R.K.J. Brown, N.I. Bohnen, K.K. Wong, S. Minoshima, K.A. Frey, Brain PET in suspected dementia: patterns of altered FDG metabolism, Radiographics 34 (3) (May 2014) 684–701, https://doi.org/10.1148/RG.343135065.

[30] S. Morbelli, et al., A Cochrane review on brain [18F]FDG PET in dementia: limitations and future perspectives, Eur. J. Nucl. Med. Mol. Imaging 42 (10) (Sep. 2015) 1487–1491, https://doi.org/10.1007/S00259-015-3098-2/METRICS.

[31] C. Cerami, et al., Brain metabolic maps in Mild Cognitive Impairment predict heterogeneity of progression to dementia, Neuroimage 7 (2015) 187–194, https://doi.org/10.1016/J.NICL.2014.12.004.

[32] V. Isella, et al., Cognitive reserve maps the core loci of neurodegeneration in corticobasal degeneration, Eur. J. Neurol. 25 (11) (Nov. 2018) 1333–1340, https://doi.org/10.1111/ENE.13729.

[33] D. Perani, et al., Validation of an optimized SPM procedure for FDG-PET in dementia diagnosis in a clinical setting, NeuroImage. Clin. 6 (2014) 445–454, https://doi.org/10.1016/J.NICL.2014.10.009.

[34] S.P. Caminiti, et al., Validation of FDG-PET datasets of normal controls for the extraction of SPM-based brain metabolism maps, Eur. J. Nucl. Med. Mol. Imaging 48 (8) (Jul. 2021) 2486–2499, https://doi.org/10.1007/S00259-020-05175-1.

[35] M.L. McHugh, Interrater reliability: the kappa statistic, Biochem. Med. 22 (3) (2012) 276–282, https://doi.org/10.11613/bm.2012.031.

[36] L. Flight, S.A. Julious, The disagreeable behaviour of the kappa statistic, Pharmaceut. Stat. 14 (1) (Jan. 2015) 74–78, https://doi.org/10.1002/PST.1659.

[37] P. Bourgeat, et al., β-amyloid PET harmonisation across longitudinal studies: application to AIBL, ADNI and OASIS3, Neuroimage 262 (Nov. 2022), 119527, https://doi.org/10.1016/J.NEUROIMAGE.2022.119527.

[38] M. Harri, T. Mika, H. Jussi, S. Nevalainen Olli, H. Jarmo, Evaluation of partial volume effect correction methods for brain positron emission tomography: quantification and reproducibility, J. Med. Phys. 32 (3) (2007) 108–117, https://doi.org/10.4103/0971-6203.35723. Jul.

[39] C.C. Meltzer, J.P. Leal, H.S. Mayberg, H.N. Wagner, J. Janies Frost, Correction of PET data for partial volume effects in human cerebral cortex by MR imaging, J. Comput. Assist. Tomogr. 14 (4) (1990) 561–570, https://doi.org/10.1097/00004728-199007000-00011.
[40] B. Alfano, M. Quarantelli, M. Comerci, A. B.-… of the 10 Th Meeting of, and U. 2004, "A New Method for Voxel Based Partial Volume Effect Correction,", ibb.cnr.it, 2004. Accessed: Sep. 08, 2023. [Online]. Available: https://www.ibb.cnr.it/papers/new_method_504be7aafa12.pdf.
[41] O.G. Rousset, Y. Ma, A.C. Evans, Correction for partial volume effects in PET: principle and validation, J. Nucl. Med. 39 (5) (May 1998) 904–911. Accessed: Sep. 08, 2023. [Online]. Available: http://www.ncbi.nlm.nih.gov/pubmed/9591599.
[42] B.M. Kandel, D.J.J. Wang, J.A. Detre, J.C. Gee, B.B. Avants, Decomposing cerebral blood flow MRI into functional and structural components: a non-local approach based on prediction, Neuroimage 105 (Jan. 2015) 156–170, https://doi.org/10.1016/J.NEUROIMAGE.2014.10.052.
[43] T. Meechai, S. Tepmongkol, C. Pluempitiwiriyawej, Partial-volume effect correction in positron emission tomography brain scan image using super-resolution image reconstruction, Br. J. Radiol. 88 (2015), https://doi.org/10.1259/BJR.20140119, 1046, Feb.
[44] J. Yang, et al., Partial volume correction for PET quantification and its impact on brain network in Alzheimer's disease, Sci. Rep. 7 (1) (2017) 1–14, https://doi.org/10.1038/s41598-017-13339-7.
[45] M. Sattarivand, M. Kusano, I. Poon, C. Caldwell, Symmetric geometric transfer matrix partial volume correction for PET imaging: principle, validation and robustness, Phys. Med. Biol. 57 (21) (Nov. 2012) 7101–7116, https://doi.org/10.1088/0031-9155/57/21/7101.
[46] P.M. Ferraro, et al., F-FDG-PET correlates of aging and disease course in ALS as revealed by distinct PVC approaches, Eur. J. Radiol. Open 9 (100394) (2022), https://doi.org/10.1016/j.ejro.2022.100394.
[47] K. Schmidt, L. Sokoloff, A computationally efficient algorithm for determining regional cerebral blood flow in heterogeneous tissues by positron emission tomography, IEEE Trans. Med. Imaging 20 (7) (2001) 618–632, https://doi.org/10.1109/42.932746. Jul.
[48] D. Albrecht, et al., Associations between vascular function and tau PET are associated with global cognition and amyloid, J. Neurosci. 40 (44) (Oct. 2020) 8573–8586, https://doi.org/10.1523/JNEUROSCI.1230-20.2020.
[49] M.A. Chappell, et al., Partial volume correction in arterial spin labeling perfusion MRI: a method to disentangle anatomy from physiology or an analysis step too far? Neuroimage 238 (Sep. 2021) 118–236, https://doi.org/10.1016/J.NEUROIMAGE.2021.118236.
[50] P. Giaccone, V. Benfante, A. Stefano, F.P. Cammarata, G. Russo, A. Comelli, PET images atlas-based segmentation performed in native and in template space: a radiomics repeatability study in mouse models, in: Lect. Notes Comput. Sci. (Including Subser. Lect. Notes Artif. Intell. Lect. Notes Bioinformatics), vol. 13373, LNCS, 2022, pp. 351–361, https://doi.org/10.1007/978-3-031-13321-3_31/FIGURES/5.
[51] F.T. Sun, R.A. Schriber, J.M. Greenia, J. He, A. Gitcho, W.J. Jagust, Automated template-based PET region of interest analyses in the aging brain, Neuroimage 34 (2) (Jan. 2007) 608–617, https://doi.org/10.1016/J.NEUROIMAGE.2006.09.022.
[52] H.J.M.M. Mutsaerts, et al., ExploreASL: an image processing pipeline for multi-center ASL perfusion MRI studies, Neuroimage 219 (Oct. 2020), 117031, https://doi.org/10.1016/J.NEUROIMAGE.2020.117031.
[53] V.T. Lehman, et al., Visual assessment versus quantitative three-dimensional stereotactic surface projection fluorodeoxyglucose positron emission tomography for detection of mild cognitive impairment and Alzheimer disease, Clin. Nucl. Med. 37 (8) (Aug. 2012) 721–726, https://doi.org/10.1097/RLU.0B013E3182478D89.
[54] A.K. Kono, K. Ishii, K. Sofue, N. Miyamoto, S. Sakamoto, E. Mori, Fully automatic differential diagnosis system for dementia with Lewy bodies and Alzheimer's disease using FDG-PET and 3D-SSP, Eur. J. Nucl. Med. Mol. Imaging 34 (9) (2007) 1490–1497, https://doi.org/10.1007/S00259-007-0380-Y/FIGURES/5. Sep.
[55] J.H. Burdette, S. Minoshima, T. Vander Borght, D.D. Tran, D.E. Kuhl, Alzheimer disease: improved visual interpretation of PET images by using three-dimensional stereotaxic surface projections, Radiology 198 (3) (1996) 837–843, https://doi.org/10.1148/RADIOLOGY.198.3.8628880.
[56] V. Isella, et al., Validity of cingulate-precuneus-temporo-parietal hypometabolism for single-subject diagnosis of biomarker-proven atypical variants of Alzheimer's Disease, J. Neurol. 269 (8) (Aug. 2022) 4440–4451, https://doi.org/10.1007/S00415-022-11086-Y.
[57] F. Nobili, et al., Automated assessment of FDG-PET for differential diagnosis in patients with neurodegenerative disorders, Eur. J. Nucl. Med. Mol. Imaging 45 (9) (2018) 1557–1566, https://doi.org/10.1007/S00259-018-4030-3. Jul.
[58] L. Presotto, T. Ballarini, S.P. Caminiti, V. Bettinardi, L. Gianolli, D. Perani, Validation of 18F–FDG-PET single-subject optimized SPM procedure with different PET scanners, Neuroinformatics 15 (2) (2017) 151–163, https://doi.org/10.1007/S12021-016-9322-9/FIGURES/4. Apr.
[59] E.J. Bacon, et al., Epileptogenic zone localization in refractory epilepsy by FDG-PET: the comparison of SPM and SPM-CAT with different parameter settings, Front. Neurol. 12 (Oct. 2021), 724680, https://doi.org/10.3389/FNEUR.2021.724680.
[60] E. Mairal, M. Doyen, T. Rivasseau-Jonveaux, C. Malaplate, E. Guedj, A. Verger, Clinical impact of digital and conventional PET control databases for semi-quantitative analysis of brain 18F-FDG digital PET scans, EJNMMI Res. 10 (1) (Nov. 2020) 1–10, https://doi.org/10.1186/S13550-020-00733-Y/FIGURES/5.